Axial load transfer for piles in sand

II: Numerical analysis

Ameir Altaee, Bengt H. Fellenius, and Erman Evgin

Department of Civil Engineering, University of Ottawa,
Ottawa, Ontario, Canada, K1N 6N5

ALTAEE, A., FELLENIUS, B.H., and EVGIN, E., 1992. Axial load transfer for piles in sand. II: Numerical analysis. Canadian Geotechnical Journal, Vol. 29, No. 1, pp. 21 - 30.

Axial load transfer for piles in sand. II. Numerical analysis

AMEIR ALTAEE, ERMAN EVGIN, AND BENGT H. FELLENIUS

Department of Civil Engineering, University of Ottawa, Ottawa, Ont., Canada K1N 6N5

Received December 28, 1990

Accepted August 15, 1991

A nonlinear finite element analysis was carried out to model the pile tests presented in the companion paper which included a new procedure to calculate the residual load in the test pile. The soil at the site consists of sand, and this second paper applies a bounding surface plasticity model in a finite element analysis to describe the behavior of the sand subjected to repeated loading. A close agreement was achieved between the calculated and measured values for the applied load versus pile head movement, load transfer, and shaft resistance in compression and tension testing. In addition, the analysis demonstrated a reduction in shaft resistance and a buildup of toe resistance with repeated loading. The finite element calculations as well as the measurements indicate that the critical-depth concept is incorrect.

Key words: pile, sand, residual load, load transfer, finite element, constitutive model.

Une analyse nonlinéaire en éléments finis a été réalisée pour modéliser les essais de pieu présentés dans l'article qui accompagne le présent article. Cette étude comprend une nouvelle procédure pour calculer la charge résiduelle dans le pieu d'essai. Le sol sur le site consiste en du sable, et ce second article applique un modèle de plasticité de surface limite dans une analyse d'éléments finis pour décrire le comportement du sable soumis à des charges répétées. Une concordance étroite a été obtenue entre les valeurs mesurées et calculées du mouvement de la tête du pieu en fonction de la charge appliquée, du transfert de charge, et de la résistance du fût dans des essais en compression et en tension. De plus, l'analyse a montré qu'il y a une réduction dans la résistance du fût et un accroissement de la résistance à la pointe avec la répétition de charge. Les calculs en élément finis de même que les mesures indiquent que le concept de profondeur critique est incorrect.

Mots clés : pieu, sable, charge résiduelle, transfert de charge, éléments finis, modélisation de comportement.

[Traduit par la rédaction]

Can. Geotech. J. **29**, 21-30 (1992)

Introduction

The load transfer behavior of the test pile described in the companion paper (Altaee *et al.* 1992*a*) was modelled using the finite element method. The analysis was performed in a continuous manner for all stages of the testing programme: the pile installation, the three compression tests in sequence, and the tension test. The numerical results from each event provided the initial state of stresses and strains in the modelling of the subsequent event.

The soil model (Bardet 1986) used in the finite element program (Altaee 1991) was chosen to account for the behavior of soil under repeated loading conditions. One set of model parameters was used for each soil layer for all stages of the numerical analysis.

To correctly model the behavior of the test pile, it was necessary to include the effect of pile installation. A new procedure was developed for the calculation of the residual stresses and strains in the soil–pile system resulting from the pile installation.

As in the conventional approach reported in the companion paper, a good agreement was obtained between the finite element results and the measurements only when the effect of pile installation was included in the analysis.

Finite element analysis

Soil model and finite element program

Soil behavior was modelled by the bounding surface plasticity model of Bardet (1986, 1987). The model employs the bounding surface concept originally proposed by Dafalias and Popov (1975). The critical state (Schofield and Wroth 1968) is taken as the bound in this model. The characteristics of soil behavior accounted for are strain hardening and strain softening, stress dilatancy, and accumulation of irreversible strains under repeated loading.

Bardet (1986, 1987) evaluated the performance of his model with respect to the behavior of Sacramento River sand and Fuji River sand. An independent assessment of capabilities of the model to simulate the behavior of a crushed quartz sand was described by Altaee *et al.* (1988) and Evgin *et al.* (1990).

Altaee *et al.* (1989, 1990, 1992*b*) have provided further validation of the model. Computations were made for the response of a sandy silt in generalized stress path tests reported by Desai and Siriwardane (1984) using a true triaxial apparatus.

The model has been implemented into a finite element program to facilitate its application to practical engineering problems (Altaee 1991). The implementation was verified by comparing the results of the finite element calculations for soil behavior in different laboratory tests with the results of calculations made by integrating the constitutive equations following the same stress or strain paths.

The finite element program was used in the analysis of two boundary value problems for further testing the validity of the soil model (Altaee *et al.* 1992*b*). In one of the boundary value problems, the load-displacement response of a model-scale footing placed on the surface of a sandy silt (Desai and Siriwardane 1984) was analyzed. The second boundary value problem was related to the behavior of Leighton Buzzard sand (Budhu and Britto 1987) in a simple shear device. The finite element results agreed well with the measured data.

Printed in Canada / Imprimé au Canada

TABLE 1. Model parameters used in the analysis

Parameter	Soil layer			
	I	II (dry)	III (moist)	IV (saturated)
Effective angle of friction (°)				
Compression	32	34	34	36
Extension	32	34	34	36
Peak	32	34	34	36
Poisson's ratio	0.3			
Aspect ratio	2.0			
Hardening parameter	1.0			
Critical void ratio at 100 kPa	0.95			
Slope of critical state line in e - ln (p) plane	0.05			
Swelling modulus	0.01			

Model parameters

The *in situ* tests reported in the companion paper (Altaee *et al.* 1992*a*) included two friction-jacket cone penetrometer tests and a standard penetration test. At present, there is no method which can provide the parameters of advanced soil models from such tests. However, since the objective of this paper is not to validate the capabilities of the constitutive model, which has already been done in the previous studies, the model parameters required for the present study were determined as follows.

The soil profile was divided into the same four layers given in Altaee *et al.* (1992*a*): an upper, 3.0 m layer of clayey silty sand and a sand layer consisting of three loose to compact layers with the same dry density but with different degree of saturation; and the upper (dry sand), lower (saturated sand), and intermediate layers (moist sand; see Table 2 in Altaee *et al.* 1992*a*). For each layer, the parameters were based on the results of the friction-jacket cone penetrometer tests and the authors' experience with the sensitivity of the model simulations to each one of its parameters. The model parameters assigned to each soil layer are shown in Table 1.

The soil parameters of the model were divided into three groups. The parameters in the first group included the effective ultimate angle of friction in compression, the effective ultimate angle of friction in extension, and the effective peak angle of friction. Since no triaxial compression and triaxial extension laboratory tests on samples from the site were available to determine these parameters, the following assumptions were made for the sand at the site. No strain-softening characteristic was assumed (when sheared in a stress path corresponding to the conventional drained triaxial test). As a result of this assumption, the peak angle of friction became equal to the ultimate angle of friction along the triaxial compression stress path. The preceding assumption regarding the two angles of friction has been found reasonable for loose to compact sand, as in the present case (Lee and Seed 1967; Tatsuoko and Ishihara 1974; Altaee *et al.* 1988; Evgin *et al.* 1989). Furthermore, the effective ultimate angle of friction in extension was assumed to be equal to that in compression.

A relationship developed by Durgunoglu and Mitchell (1975) between effective angle of friction and cone resistance for different vertical effective stresses was used to estimate the peak effective angle of friction. According to this method, the angle of friction varied between 32 and 36° for the sand below the 3 m upper layer. This method gives a reasonable lower bound of angle of friction for sands with the quartz fraction dominating as reported by Robertson and Campanella (1983). No further refinement was attempted to modify the effective angle of friction. Thus, a value of 34° was assigned to the second and third soil layers, whereas a value of 36° was used for the last soil layer, as shown in Table 1. For the 3 m upper silt and sand layer, an estimated value of effective angle of friction of 32° was used.

The second group of parameters included the Poisson's ratio, which was assigned a value of 0.3. This is a typical value used by others (e.g., Bardet 1987). The second parameter in this group was the hardening parameter, which was assigned a value of 1. This parameter has little effect on the overall performance of the model. The third parameter in this group was the bounding surface aspect ratio, which was assigned a value of 2.0. Previous experience with the model has indicated that an aspect ratio equal to 2.0 is suitable for loose to compact sand, as in the present case.

The parameters in the third group are related to the compressibility of the soil, and they were selected from the literature for similar soils.

Using the model parameters in Table 1, the behavior of the saturated sand was simulated in an isotropic compression test and three conventional triaxial drained compression tests at different confining pressures. Figure 1 shows the simulated isotropic stress versus volumetric strain relation in a loading and unloading path. The simulations of the conventional triaxial tests are shown in Fig. 2. The general trends in these simulated cases are similar to those obtained from actual testing of different types of loose sand (Lee and Seed 1967; Tatsuoka and Ishihara 1974; Altaee *et al.* 1988; Evgin *et al.* 1989).

Initial stresses in the soil

Initial stresses are important for the nonlinear analysis of soil masses or soil–structure interaction problems. Previous finite element studies of piles (e.g., Desai and Holloway 1972; Desai 1974) have not included the presence of residual load. Instead, they back-calculated the initial horizontal stresses in the soil from the results of analysis of field loading tests. This means that the horizontal stresses at failure were assigned as the initial horizontal stresses in the analysis of the loading tests. Furthermore, to get the calculations to

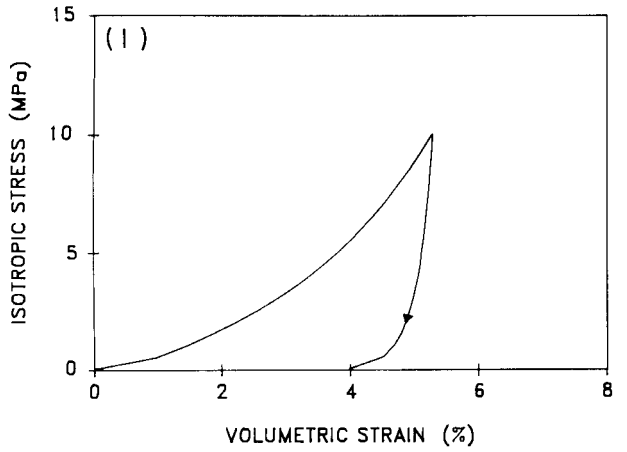

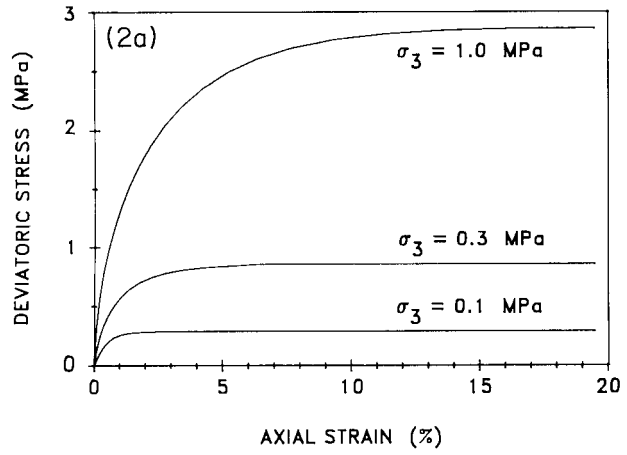

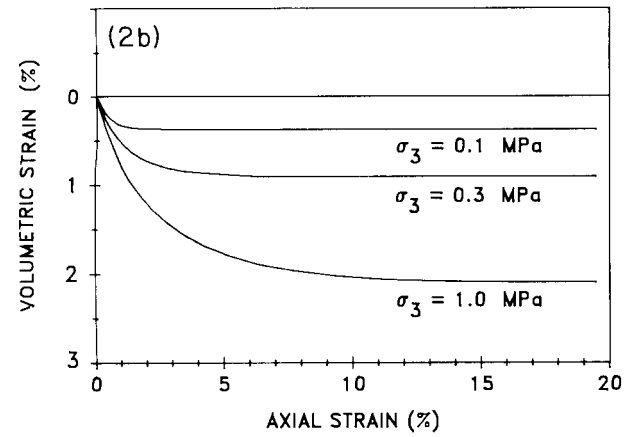

FIG. 1. Simulated isotropic compression test. FIG. 2. Simulated drained triaxial compression tests. (*a*) Deviatoric stress vs. axial strain. (*b*) Volumetric strain vs. axial strain.

match the shaft resistance measured both in compression and in tension, different initial horizontal stresses were used in the analysis of compression loading and tension loading.

In the present work, in contrast, the initial soil stresses employed in the analyses are those before the pile installation (calculated using the densities and the groundwater table location reported in Altaee *et al.* 1992*a*).

The calculations assumed that the soil was normally consolidated. Jaky's equation was used to calculate the coefficient of earth pressure at rest, K_o. Values of K_o of 0.47, 0.44, 0.44, and 0.41 were obtained for the first, second, third, and fourth soil layers, respectively. The initial (before pile driving) effective horizontal stress at a specified depth was then calculated as K_o times the effective overburden stress at that depth. Since the soil was in at-rest condition, no shear stresses were present in horizontal and vertical planes.

Finite element idealization of soil–pile system

The pile–soil system was modeled using an axisymmetric idealization. The selection of the mesh was based on convergence requirements (Desai and Abel 1972). A parametric study was carried out to find the optimum mesh size. Further requirements in the mesh size showed negligible differences in the computed load versus pile head movement response of the test pile. Far-field soil boundaries were selected using the same principle.

The length and axial stiffness of the idealized pile were of course the same as those of the test pile. However, to have an axisymmetric idealization of the pile–soil system, the square test pile had to be approximated as a circular pile. The selection of a representative diameter, however, posed a difficulty because finding a circular pile with the same toe and shaft area as the square test pile is not possible. Three practical options were considered in the selection of the diameter. One option was to select a circular diameter of 362.8 mm, which gave the same shaft area as the test pile but exceeded the actual toe area by 27.3%. A second option was to select a circular diameter of 321.6 mm, which satisfied the equality of the toe area but gave a shaft area 11.4% smaller than that of the actual pile. The third option, which was between the first two extreme cases, was to select a circular diameter of 340 mm, toe area 11.7% larger than that of the test pile, and shaft area 6.4% smaller than that of the test pile.

The use of any of the above options requires adjustments in the total load and total shaft resistance or total toe resistance. However, if these adjustments are made proportional to the ratios of the toe or shaft areas of the test pile and the analyzed pile, the potential influence of the scale effects cannot be accurately compensated for. In the present finite element analysis, the shaft resistance and toe resistance were adjusted by the following method: the finite element analyses were carried out for three, 11.0 m long piles with the aforementioned diameters (362.8, 340.0, and 321.6 mm). The results were plotted to show the ultimate shaft resistance as a function of the shaft area and the ultimate toe resistance as a function of the toe area.

Modelling the effect of pile installation

Previous work

The literature contains the following studies of piles in sand which simulate the effect of pile installation and development of residual load.

Holloway *et al.* (1978, 1979) presented a numerical procedure using a finite difference formulation to simulate the behavior of a pile subjected to one-dimensional impact loading. This procedure enables the determination of residual stresses induced by the driving. A computer program called DUKFOR was developed, where pile driving was modeled using Smith's (1960) one-dimensional wave propagation equation. The analysis proceeds with modelling a series of single blows to establish the residual stress rate at the end of driving. After completing this stage, the DUKFOR analysis

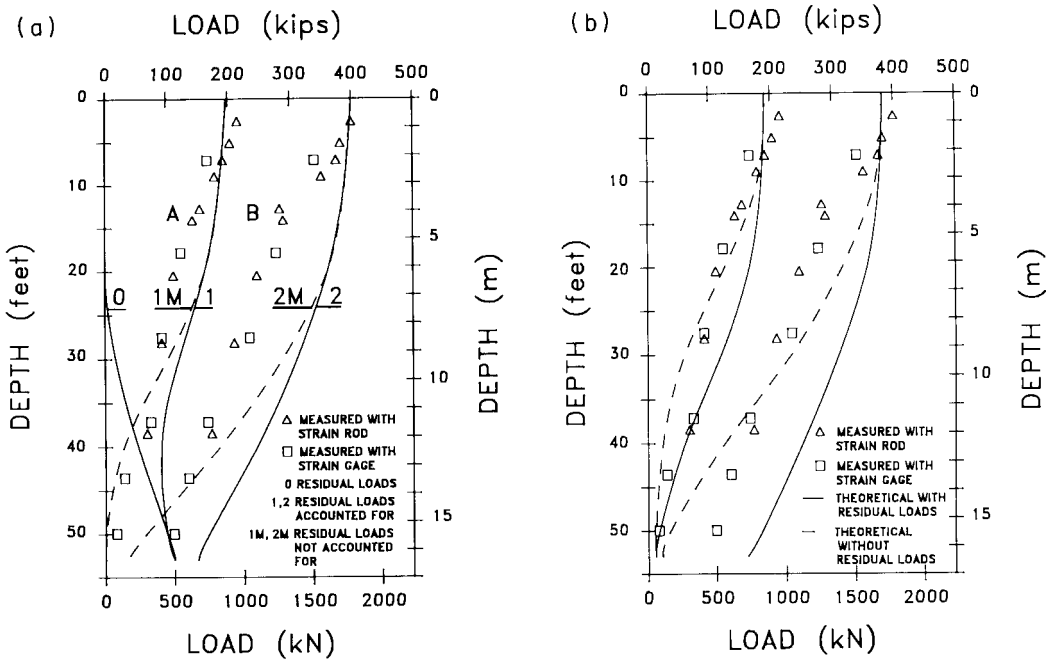

FIG. 3. Load distribution in pile LD4TP2. (*a*) Modified after Holloway *et al.* (1978). (*b*) Modified after Poulos (1987).

continues to model the behavior of the pile subjected to a compression or tension loading test.

Holloway *et al.* (1978, 1979) used the computer program to calculate the behavior of one of the piles at Lock and Dam No. 4 of the Arkansas River Navigation Project. Figure 3*a* compares the computed and measured pile load distribution data during a compression test. Curve 0 represents the computed residual load immediately following driving. Curves 1 and 2 represent the computed values for the actual load (includes residual load) distribution in the pile for two different loads at the pile head. The measured load distributions (shown as data points) corresponding to these loads are marked by A and B. For the purpose of drawing the computed corresponding curves, the computed residual load (curve 0) is subtracted from curves 1 and 2. Curves 1M and 2M represent the computed values of Holloway *et al.* (1978, 1979) for the measured data represented by curves A and B.

The curves presented in Fig. 3*a* indicate some discrepancy between the computed and the measured load transfers. The discrepancy is larger for the higher pile head load.

More recently, Poulos (1987) presented a method for the estimation of the residual stresses in single piles installed by "driving" or "jacking." The boundary element procedure described by Poulos and Davis (1980) was used. This method replaces the dynamic analysis of Holloway *et al.* (1978, 1979) by a static analysis to estimate residual load. Poulos (1987) applied his method to compute the load transfer in the same pile used by Holloway *et al.* (1978). The results are shown in Fig. 3*b*.

Both Poulos (1987) and Holloway (1978, 1979) require input parameters that are determined from a failure state. These parameters are ultimate unit shaft resistance along the pile for both tension and compression loading and the limiting toe resistance. The determination of these values depends on the magnitude and distribution of the residual load in the pile, which themselves are not known. Neither

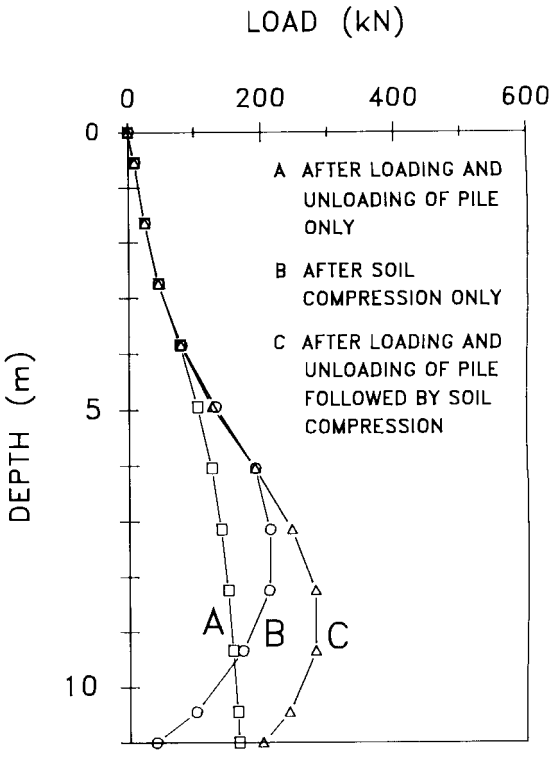

FIG. 4. Computed residual loads as a result of pile installation.

method includes the effect of soil compression on the residual load.

Present work

In the present work, a new procedure is used to determine the magnitude and distribution of residual load in a test pile. The procedure differentiates between residual loads developed in piles in sand as a result of the installation method (whether pushed in, buried, or driven; the first two methods are used extensively in laboratory testing).

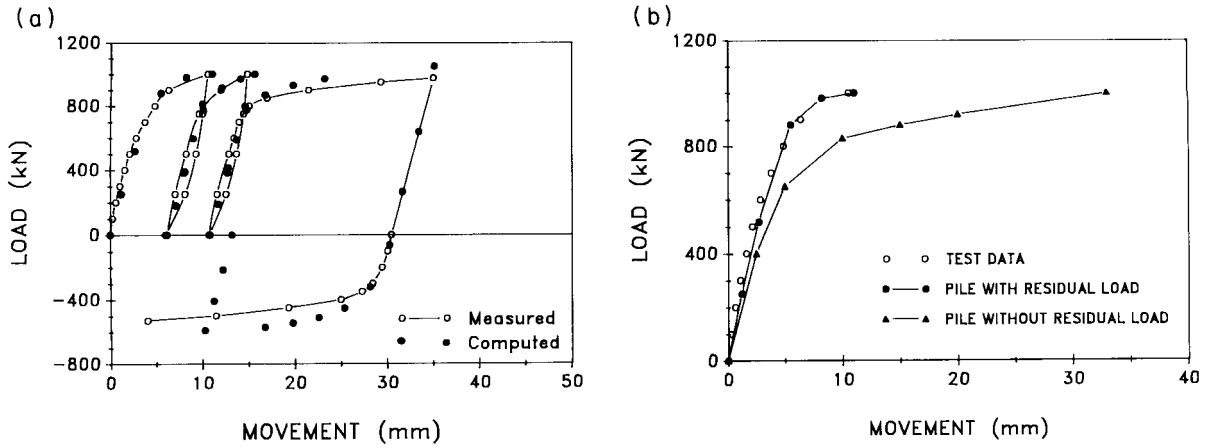

FIG. 5. Applied load vs. pile head movement response. (*a*) Calculations vs. measurements. (*b*) Pile with residual load vs. stress-free pile.

For piles pushed into sand, residual load in the pile caused by the installation is modelled by loading the pile in compression (the pile being at its final embedment depth) until failure and then unloading it back to zero load at its head. This type of residual load development is denoted type A. The axial load remaining in the pile after complete unloading is considered to be the residual load in the pile. A typical case of pile installation in this manner is reported by Chan and Hanna (1980).

Two aspects control the distribution of type A residual load in the pile: first, the relative magnitude between the total toe resistance and the total shaft resistance, and, second, the length and stiffness of the pile. If the pile is long and the ultimate toe resistance is larger than the ultimate shaft resistance, residual load in the pile will increase all the way to the pile toe, and a significant residual toe resistance is developed. If, on the other hand, the pile is short and stiff, the magnitude of elastic rebound of the pile may be too small to do much more than reverse the direction of movement, that is, the mobilized shear resistance is sufficient to eliminate the existing positive shaft resistance, but the movement is insufficient to build up negative skin friction. In contrast with the long flexible pile, a short stiff pile will have only a small amount of residual load.

For piles buried into the soil (e.g., Hanna and Tan 1973; Tan and Hanna 1974), the residual load (denoted type B) in the pile is calculated by simulating an incremental buildup of soil around the pile. This type can also be simulated by letting the surrounding soil compress around the pile.

Type B residual load is associated with only a small residual toe resistance also for the long pile, and therefore the point of force equilibrium (neutral plane) will always be some distance above the pile toe.

A bored pile more closely resembles the buried pile situation, and type B residual load, therefore, is representative of a bored pile. However, the residual load for a driven pile is more complicated. When the effect of the last blow has gone, at first, the residual load is similar to the type A condition. However, starting immediately and for some time (short or long) after driving, the soil recovers from the installation disturbance, and additional downward movement is built up in the soil relative to the pile, adding load to the existing type A residual load. This can be simulated by combining the types A and B effects: the type B simulation uses the end result of type A as its starting point. It should be realized that this is not a superpositioning of the two types of residual load distribution.

Computed residual load in the subject test pile

The procedure outlined above was used to compute the magnitude and distribution of the residual load in the test pile considered in this study.

Curve A in Fig. 4 represents the computed type A residual load in the test pile as installed by pushing. It represents the residual load due to the release of the load at the pile head upon unloading. The numerical simulation was achieved by applying increments of downward displacement at the pile head until there was no appreciable additional resistance to further movement (soil failure), whereupon the load at the pile head was removed. The resulting distribution of the residual load (curve A) is similar to those calculated by Holloway *et al.* (1978, 1979) and Poulos (1987) shown in Figs. 3*a* and 3*b*. The main similarity is that the maximum residual load is located at the pile toe and that, therefore, negative skin friction occurs over the full pile length.

Curve B in Fig. 4 shows the computed type B residual load in the test pile as installed by burying, taking an unloaded pile as the starting condition. The analysis proceeded in a manner similar to the simulation of the type A residual load but with the weight of an upper 1.5 m thick soil layer excluded from the analysis. Then, to produce the type B residual load, the weight of this upper soil layer was added in increments combined with the pile head being free to move. The selection of 1.5 m thickness for the upper soil layer was based on a preliminary analysis in which the thickness of the soil layer was varied to study the effect on the magnitude and distribution of residual load.

Curve C in Fig. 4 shows the computed type C residual load in the test pile as described above. The numerical analysis was carried out combining the type A and type B approaches, type B being performed immediately after type A using the type A condition of stress and strain as the starting condition.

Numerical results

Applied load versus pile head movement

The finite element computations of the applied load versus pile head movement for all four tests are shown in Fig. 5*a*.

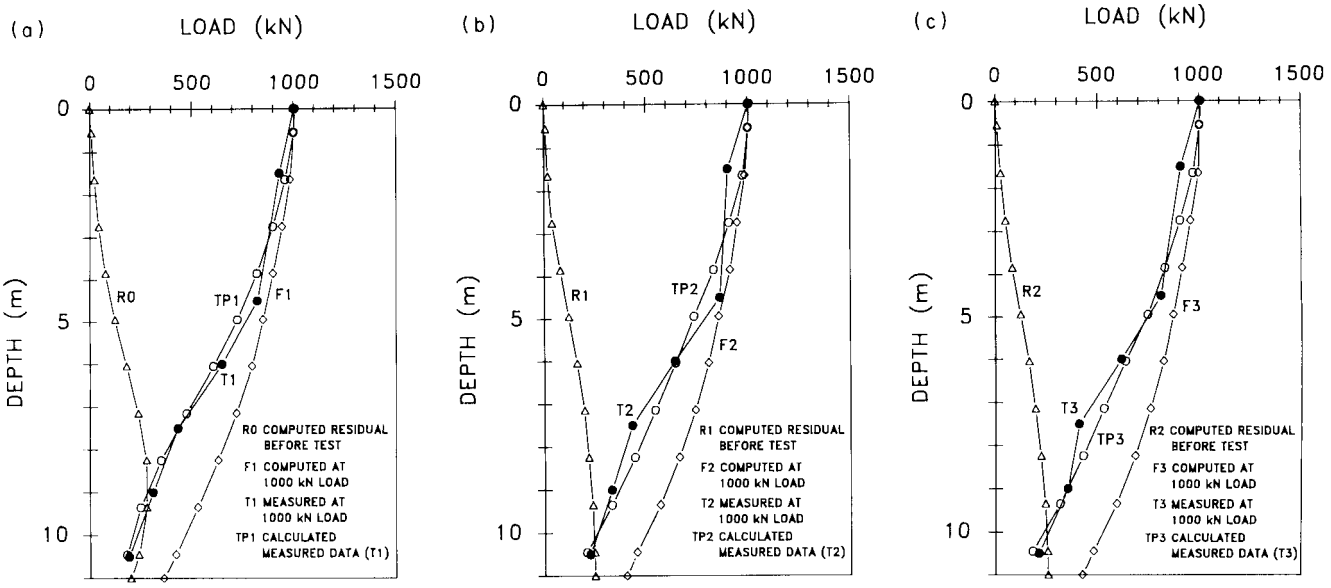

FIG. 6. Distribution of axial load in the (*a*) first, (*b*) second, and (*c*) third compression tests.

The figure also shows the measured values. The computations for the third compression loading were stopped at a displacement of about 35 mm rather than continuing to 120 mm as recorded in the actual test (Altaee *et al.* 1992*a*). After 35 mm displacement of the pile head, the pile was unloaded and the analysis of the tension test started.

The applied load versus pile head movement data from the first compression test were used in the selection of the swelling modulus. The agreement between the computed and measured values of applied load versus pile head movement in the first compression test is, therefore, imposed. However, as shown in Fig. 5*a*, a very good agreement exists between the computed values and the actual measurements throughout the remaining three loading tests.

The finite element computations for the applied load versus pile head movement in the tension test gave a slightly stiffer response compared with the actual measurements. This difference is attributed, in part, to the use of the same modulus of elasticity for the pile material in tension and compression. Since the actual modulus of elasticity in tension is slightly lower than that in compression, the elastic elongation of the pile was underestimated in the finite element calculations of the tension loading test.

The maximum load measured in the tension test was 580 kN (including the weight of the pile), whereas the finite element calculations indicated a maximum load of about 600 kN (including the weight of the pile), overestimating the tension failure load. However, at the time of the tension test, the groundwater table had risen from 6.4 to 5.0 m. This resulted in the reduction of effective stresses, which in turn reduced the shaft resistance. In contrast with the treatment used in Altaee *et al.* 1992*a* the effect of the changes in the groundwater table was not accounted for in the present calculations.

Effect of residual load on applied load versus pile head movement

Residual load in a pile affects its load–movement response. This is demonstrated in Fig. 5*b* for the present test pile. The figure compares the computed applied load versus pile head movement in the first compression test for the test pile with initial residual load (same as that shown in Fig. 5*a*) and the applied load versus pile head movement of the test pile without residual load prior to the loading test. Both analyses were carried to loads of 1000 kN. The figure illustrates that a pile–soil system with no residual load requires larger movements to mobilize the same load than for a pile–soil system with residual load. This difference is because the residual load preloads the pile toe.

The results shown in Fig. 5*b* are in agreement with the laboratory observations made by Hanna and Tan (1973) on small-scale instrumented piles tested in sand, the results of the analytical studies by Poulos (1987), and the results of the analysis of some case histories reported by Vesic (1977). Both the experimental and analytical results reported in the literature show that a stiffer response is to be expected (i.e., smaller head movement is required to mobilize the same resistance) when piles with residual load are tested in compression as opposed to piles with no residual load. This observation can be used to evaluate the consistency of any numerical analysis of axially loaded piles. Since the presence of residual load affects the applied load versus pile head movement response of a pile, no agreement should be expected between the results of the numerical analysis and the actual measurements if the residual load is not included in the analysis. In fact, if a good agreement is achieved without considering the residual load, this indicates that an error is made in the input of soil stiffness and (or) that nonrepresentative initial horizontal stresses in the soil are assumed in the analysis.

Load transfer

In the present tests, the gages were zeroed at the start of each loading test. Consequently, the loads measured in the pile do not represent the true loads. In the numerical analysis, the measured load distributions were calculated by subtracting the computed residual load from the load distributed along the pile (explained further in the companion paper). Computed distribution curves were compared with those obtained from the field measurements for the three compression loading tests.

The load values measured in the pile during the first com-

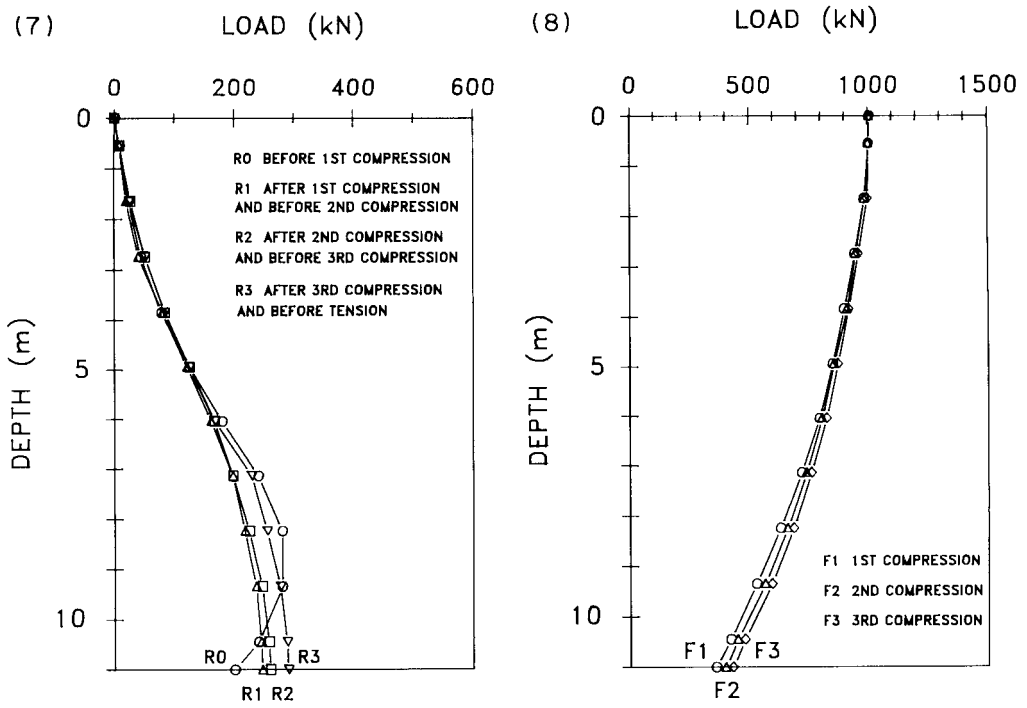

FIG. 7. Distribution of residual load at different stages of testing. FIG. 8. Distribution of axial load in the pile at the end of each compression test.

pression test are labeled T1 in Fig. 6*a*. The values computed from the finite element analyses for the same applied load at the pile head are shown in the figure as curve F1 and include residual load effects. The computed residual load (type C) in the pile prior to the first loading test is labeled R0. This residual load is the result of the pile installation. Curve TP1 is the computed "measured load distribution" obtained by subtracting the computed residual load (curve R0) from the load shown by curve F1. The agreement between the finite element calculations, curve TP1, and the test results, curve T1, is excellent.

Similar agreements are obtained in the analyses of the second and third compression tests. The results of these comparisons are provided in Figs. 6*b* and 6*c*. As shown in these figures, the residual loads used in the analysis of all tests are different from each other. This is because the residual load at the pile toe increases by each loading event, as shown in Fig. 7.

Effects of repetitive loading on load transfer

Each test showed an increase in the load carried by the pile toe and reduction in the load carried by the pile shaft, as shown in Fig. 8. The figure compares the load transfer in the three compression tests for 1000 kN load at the pile head. The curves labeled F1, F2, and F3 correspond to the first, second, and third compression tests, respectively.

The computed toe resistances for each of the three compression tests were 360, 400, and 430 kN and the shaft resistances were 640, 600, and 570 kN, respectively. The reduction in the shaft resistance is further illustrated by plotting the shear stresses on vertical planes in the soil elements adjacent to the pile shaft as shown in Fig. 9*a*. The shear stress along the pile shaft decreased with each loading event. This reduction in the shear stress was higher in the vicinity of the pile toe compared with the reductions at other locations.

Gradual degradation of shaft resistance has been observed before, e.g., Chan and Hanna (1980), Boulon *et al.* (1980), Nauroy *et al.* (1985), Puech and Jezequel (1980), and Turner and Kulhawy (1989). These authors attributed the observed degradation of the shaft resistance to a potential progressive decrease in the horizontal (lateral) stress in the soil. Indeed, the present study indicates that the horizontal stress decreases from test to test as shown in Fig. 9*b*. Figure 9*b* shows the variation of the horizontal stress in the soil elements adjacent to the pile shaft at a 1000 kN load on the pile head for all three compression tests. The variation in horizontal stress is similar to that of shear stresses shown previously in Fig. 9*a*.

Tension loading test

No information regarding load transfer is available for the tension loading test for the reasons discussed in Altaee *et al.* 1992*a*. However, load–movement data were available as presented, and it was compared with the numerical calculations in Fig. 5*a*.

The numerical results of the tension test were also used to compare the calculated ultimate shaft resistance of the test pile in tension and compression.

Figure 10 gives the ultimate shear stresses on the vertical planes passing through the soil elements adjacent to the pile shaft. Curve F4 is related to the tension test, and curve F3 to the third compression test. The shear stress values are similar along the whole pile length, and this suggests that, for all practical purposes, the ultimate shaft resistance in compression is equal to that in tension for this test pile.

The computed load transfer in the tension test obtained from the finite element analysis is shown in Fig. 11. Before the tension test started, the pile was under compression due to the residual load that remained after the third compression test. The distribution of this residual load is shown as curve R3. This distribution implies that, before the tension

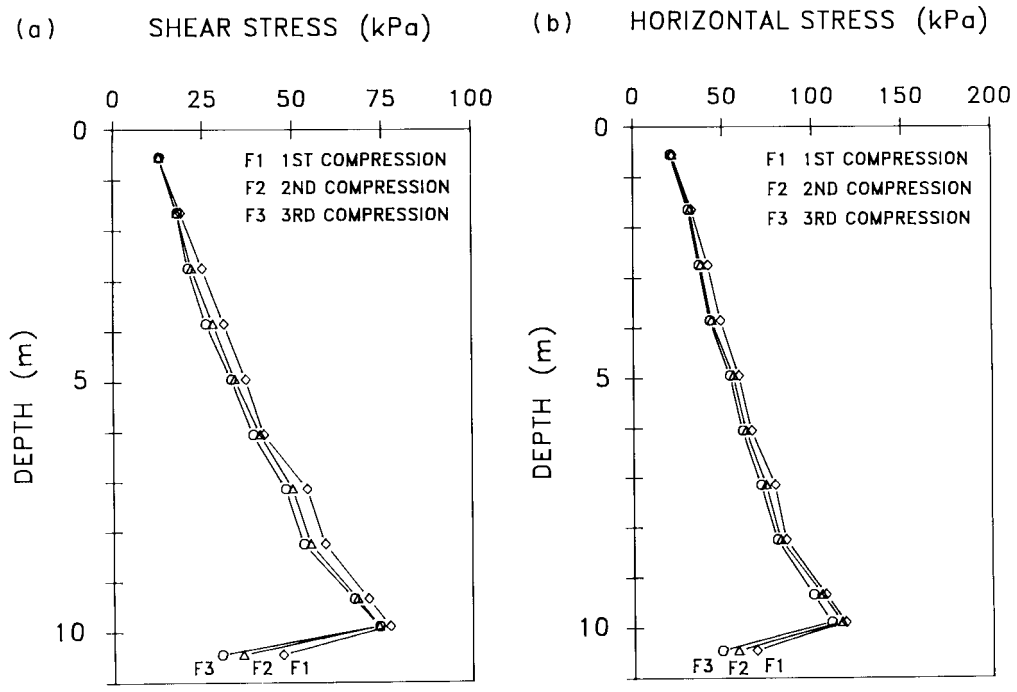

FIG. 9. Distribution of (*a*) shear stresses and (*b*) horizontal stresses in the soil adjacent to the pile shaft in three compression tests.

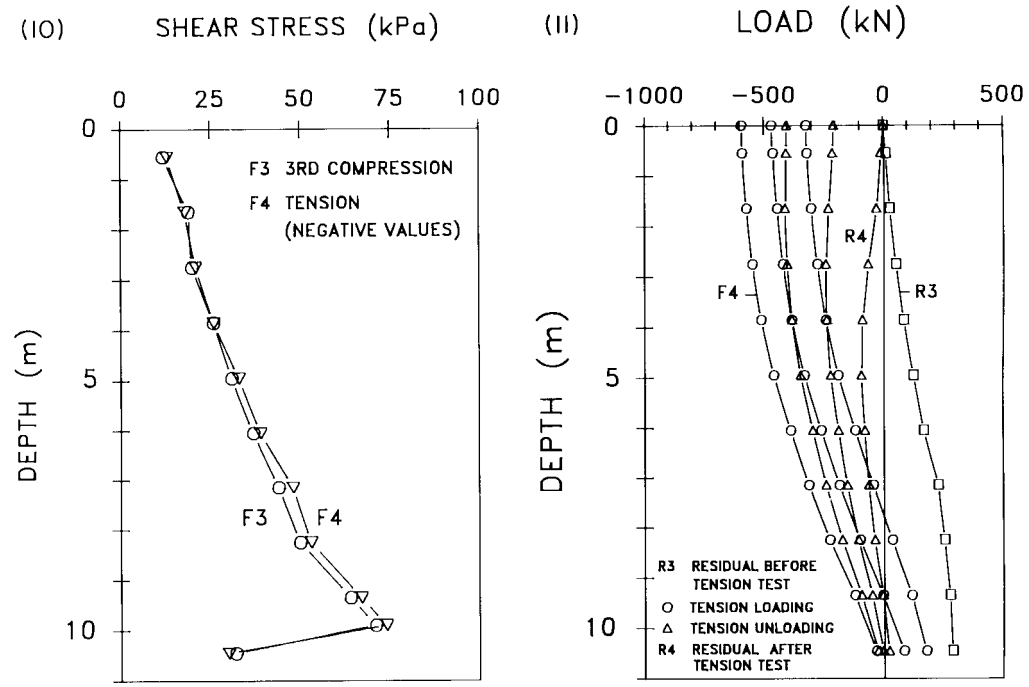

FIG. 10. Distribution of shear stresses in the soil adjacent to the pile shaft in the third compression test and the tension test.
FIG. 11. Distribution of axial load in the pile in the tension test.

test, the shear strength of the soil along the upper portion of the pile is already mobilized due to the presence of the residual load. Furthermore, the pile has a significant residual load at its toe.

With increasing tension load at the pile head, the soil along the lower portion of the pile starts to mobilize more and more shaft resistance, whereas unloading of the residual load at the toe continues. At the maximum tension load, the distribution of the axial load in the pile is shown as curve F4.

With unloading, the load transfer is changing at each loading level. At the complete unloading, the distribution of the axial load in the pile is shown in Fig. 11 as curve R4. This curve represents the load remaining in the pile after the tension test. Note that the residual toe load diminishes to zero at the end of the test. It is of interest to note that a significant amount of residual *tension* load is produced as a result of the tension test. Such residual load at the end of the tension test was assumed not to exist in the Hunter and Davisson (1969) method of interpretation of loading test

data from instrumented piles. Neglecting the tension residual load affects the shape of the distribution of the unit shaft resistance in compression by the Hunter and Davisson method.

Conclusions

The results of the finite element analysis agree very well with the measured data and, also, with the results of the conventional method of analysis presented in Altaee *et al.* 1992*a*. Throughout the testing programme, this agreement is noticeable in the applied load versus pile head movement response as well as in the load transfer along the pile shaft. No such agreement can be achieved if the pile is assumed stress free before the start of static testing.

Using the residual load computed as an integral part of the analysis eliminates the need for the critical depth concept to explain the measured data.

The test results and the results of the finite element analysis demonstrate the importance of loading history on the development of residual load.

A gradual increase in the residual toe load develops with each repeated compression loading. This increase is due to the accumulation of the downward toe movement at the end of each load repetition.

The calculated values of the ultimate total shaft resistance in tension and compression loading are equal. In addition, there is no difference in the distribution of the unit shaft resistance during the compression and tension loading.

The ultimate shaft resistance degrades with each repetition of compression loading. Reduction in horizontal stresses is observed from the numerical computation, which supports the hypothesis that the observed degradation of shaft resistance is due to a reduction in horizontal stresses. The degradation of the shaft resistance is accompanied by an increase in the degree of mobilization of the toe resistance.

A significant amount of residual tension load is calculated in the pile at the end of unloading from the tension loading.

Acknowledgements

The numerical part of this work was carried out at the University of Ottawa, Department of Civil Engineering, and was financially supported by the Natural Sciences and Engineering Research Council of Canada. The analyses were carried out using the main computer of the University of Ottawa.

Altaee, A. 1991. Finite element implementation, validation, and deep foundation application of a bounding surface plasticity model. Ph.D. thesis, University of Ottawa, Ottawa, Ont.

Altaee, A., Evgin, E., and Fellenius, B.H. 1988. Modelling sand behavior for cyclic loading. Proceedings, 41st Canadian Geotechnical Conference, Waterloo-Kitchener, Ont., pp. 326–335.

Altaee, A., Evgin, E., and Fellenius, B.H. 1989. An application of a bounding surface plasticity model. Proceedings, 42nd Canadian Geotechnical Conference, Winnipeg, Man., pp. 169–176.

Altaee, A., Evgin, E., and Fellenius, B.H. 1990. Finite element applications of a bounding surface plasticity model. Journal of Mathematical and Computer Modelling, **14**: 909–914.

Altaee, A., Fellenius, B.H., and Evgin, E. 1992*a*. Axial load transfer for piles in sand. I. Tests on an instrumented precast pile. Canadian Geotechnical Journal, **29**: 11–20.

Altaee, A., Evgin, E., and Fellenius, B.H. 1992*b*. Finite element validation of a bounding surface plasticity model. Computers and Structures. (In press.)

Bardet, J.P. 1986. Bounding surface plasticity model for sands. ASCE Journal of the Engineering Mechanics Division, **112**: 1198–1217.

Bardet, J.P. 1987. Bounding surface modelling of cyclic sand behavior. *In* Proceedings, Workshop on Constitutive Laws for the Analysis of Fill Retention Structures. *Edited by* E. Evgin. Energy, Mines and Resources Canada Publication 0825-25-6-3, pp. 1–19.

Boulon, M., Desrues, J., Foray, P., and Forgue, M. 1980. Numerical model for foundation under cyclic loading. Proceedings, International Symposium on Soils Under Cyclic and Transient Loading, Swansea, United Kingdom, vol. 2, pp. 681–694.

Budhu, M., and Britto, A. 1987. Numerical analysis of soils in simple shear devices. Soils and Foundations, **27**: 31–41.

Chan, S.F., and Hanna, T.H. 1980. Repeated loading on single piles in sand. ASCE Journal of the Geotechnical Engineering Division, **106**: 171–188.

Dafalias, Y.F., and Popov, E.P. 1975. A model of nonlinearly hardening materials for complex loadings. Acta Mechanica, **21**: 173–192.

Desai, C.S. 1974. Numerical design-analysis for piles in sands. ASCE Journal of the Geotechnical Engineering Division, **100**: 613–635.

Desai, C.S., and Abel, J.F. 1972. Introduction to finite element methods. Van Nostrand Reinhold Company Inc., New York.

Desai, C.S., and Holloway, D.M. 1972. Load-deformation analysis of deep pile foundations. Proceedings, Symposium on Applications of the Finite Element Method in Geotechnical Engineering, United States Army Engineers Waterways Experiment Station, Vicksburg, Miss.

Desai, C.S., and Siriwardane, H.J. 1984. Constitutive laws for engineering materials. Prentice-Hall Inc., Englewood Cliffs, N.J.

Durgunoglu, H.T., and Mitchell, J.K. 1975. Static penetration resistance of soils. Proceedings of the ASCE Conference on In-situ Measurement of Soil Properties, Raleigh, N.C., vol. 1, pp. 151–188.

Evgin, E., Amor, F.B., Altaee, A., Lord, S., and Konuk, I. 1989. Effect of an oil spill on soil properties. *In* Proceedings, 8th International Conference on Offshore Mechanics and Arctic Engineering. *Edited by* J.S. Chung, C.P. Ellinas, B.J. Natvig, J. Wardenier, and T.R. Penney. American Society of Mechanical Engineers, New York, vol. IV, pp. 715–720.

Evgin, E., Altaee, A., Lord, S., and Konuk, I. 1990. Modelling the behavior of an oil saturated sand. *In* Proceedings, 9th International Conference on Offshore Mechanics and Arctic Engineering. *Edited by* O.A. Ayorinde, N.K. Sinha, and D.S. Sodhi. American Society of Mechanical Engineers, New York, vol. IV, pp. 31–37.

Faruque, M.O., and Desai, C.S. 1985. Implementation of a general constitutive model for geological materials. International Journal for Numerical and Analytical Methods in Geomechanics, **9**: 415–436.

Hanna, T.H., and Tan, R.H.S. 1973. The behavior of long piles under compressive loads in sand. Canadian Geotechnical Journal, **10**: 311–340.

Holloway, D.M., Clough, G.W., and Vesic, A.S. 1978. The effects of residual driving stresses on pile performance under axial load. Proceedings, 10th Offshore Technology Conference, Houston, Tex., vol. 4, pp. 2225–2236.

Holloway, D.M., Clough, G.W., and Vesic, A.S. 1979. A rational procedure for evaluating the behavior of impact-driven piles. *In* Behavior of deep foundations. *Edited by* R. Lundgren. American Society for Testing and Materials, Special Technical Publication 670, pp. 335–357.

Hunter, A.H., and Davisson, M.T. 1969. Measurements of pile load transfer. Proceedings, Symposium on Performance of Deep